CHEMISTRY OF MATERIALS

pubs.acs.org/cm

Article

Phosphorene Degradation: Visualization and Quantification of Nanoscale Phase Evolution by Scanning Transmission X-ray Microscopy

Weihan Li, Zhiqiang Wang, Feipeng Zhao, Minsi Li, Xuejie Gao, Yang Zhao, Jian Wang, Jigang Zhou, Yongfeng Hu, Qunfeng Xiao, Xiaoyu Cui, Mohammad Javad Eslamibidgoli, Michael. H. Eikerling, Ruying Li, Frank Brandys, Ranjith Divigalpitiya, Tsun-Kong Sham,* and Xueliang Sun*

Cite This: *Chem. Mater.* 2020, 32, 1272−1280

Read Online

ACCESS | Metrics & More | Article Recommendations | Supporting Information

ABSTRACT: Phosphorene, single- or few-layered black phosphorus, has been rediscovered as a promising two-dimensional material owing to its unique optical, thermal, and electrical properties with potential applications in optoelectronics, nanoelectronics, and energy storage. However, rapid degradation under ambient condition highly limits the practical applications of phosphorene. Solving the degradation problem demands an understanding of the oxidization process. We, for the first time, apply synchrotron-based X-ray photoelectron spectroscopy (XPS), X-ray absorption near-edge structure (XANES), and scanning transmission X-ray microscopy (STXM) for the nanoscale chemical imaging of phosphorene degradation. Through these methods, we have identified chemical details of the morphological effect and clarified thickness and proximity effects, which control the oxidization process. Furthermore, the entire oxidization process of phosphorene has also been studied by in situ XPS and XANES, showing the step-by-step oxidization process under the ambient condition. Theoretical calculations at the density functional theory level support experimental findings. This detailed study provides a better understanding of phosphorene degradation and is valuable for the development of phosphorene-based materials.

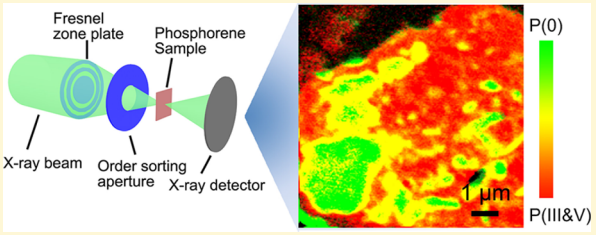

1. INTRODUCTION

Recently, phosphorene, single- or multi-layered black phosphorus (BP), has been rediscovered as a two-dimensional (2D) electronic material and has received intensive attention in research since its first isolation in 2014, showing an orthorhombic structure with puckered double layers.[1−3] The renaissance of phosphorene was driven by a unique set of properties, including the tunable direct band gap (from 0.3 eV of bulk BP to 2.0 eV of the monolayer structure) and high carrier mobility (up to 1000 $cm^2\ V^{-1}\ s^{-1}$ observed experimentally and up to 10,000−26,000 $cm^2\ V^{-1}\ s^{-1}$ predicted by theory).[3−7] In addition, the anisotropic in-plane properties of phosphorene, such as optical, thermal, and electrical properties, make it promising for applications in optoelectronics, nanoelectronics, and energy storage.[8−12] However, the rapid degradation of phosphorene under the ambient condition impedes its practical applications.[13,14]

The degradation process is related to two main effects, environmental effect (e.g., light, oxygen, and water) and morphological effect (e.g. thickness and oxidized regions in the vicinity); in the ambient, degradation occurs from several hours to days.[15,16] Upon exposure to light, oxygen defects are initially formed which then react with water to form a mixture of oxides and phosphoric acid.[17−19] While the thickness (i.e., number of layers) of the material determines its band structure and oxidization mechanism, the existing regions already oxidized will affect the oxidation kinetics of the unoxidized region in the vicinity, expanding the local oxide layer thickness and expediting the degradation process.[14,20] Several groups have applied optical microscopy,[15,21] atomic force microscopy (AFM),[16,18,22] and Raman spectroscopy[17] to track morphology changes during phosphorene degradation under different environments, showing the gradual transformation from a smooth surface to a rough surface with growing oxide protrusions and bubbles.

To understand the chemical reaction behind the morphology change, X-ray photoelectron spectroscopy (XPS),[23,24] electron energy loss spectroscopy (EELS),[22] anion-exchange chromatography,[25] and nuclear magnetic resonance (NMR) studies[26] have been carried out to track the variation of valence states and chemical compositions. Furthermore, quantum mechanical calculations based on density functional theory

Received: November 20, 2019
Revised: January 15, 2020
Published: January 15, 2020

https://dx.doi.org/10.1021/acs.chemmater.9b04811
Chem. Mater. 2020, 32, 1272−1280

(DFT) have been performed to develop an atomistic understanding of the processes leading to oxide formation and phosphorene degradation.[19,27] In addition to environmental effects, the morphological effect has also been investigated using AFM, scanning Raman microscopy (SRM), and infrared scattering scanning near-field microscopy (IR s-SNOM).[16,20,28] In one study, it was found that the thinner regions of phosphorene show higher degradation rate (i.e., thickness effect), tracked by the AFM and SRM, while the oxidized phosphorene accelerates the degradation of adjacent regions (i.e., neighboring effect), as also suggested by the phenomenological modeling of IR s-SNOM result. Nevertheless, these three reports of morphological effect study mainly focused on the variation of morphology, and few reports presented a clear and detailed picture from a chemical point of view.[17] In another study, Martel et al. used transmission electron microscopy (TEM) to track the thickness information by high-angle annular dark field contrast and the oxidation states by EELS images, presenting the thickness effect on phosphorene degradation.[17] However, the energy resolution of EELS images is limited, showing inadequate chemical sensitivity to distinguish different oxidation states.[29] Considering the previous works, the main challenge to realize detailed analysis and to obtain a clear conclusion of morphology effect is the ability to image the local morphology and chemical states at nanoscale resolution.

As sensitive methods to characterize oxidation states, synchrotron-based XPS and X-ray absorption fine structure, especially X-ray absorption near-edge spectroscopy (XANES), are two of the most precise techniques to clarify the chemical states and the coordination chemistry.[30−32] In addition, absolute thickness information of samples can be calculated based on the edge jump, if XANES is conducted on an individual nanosheet through the transmission mode.[33,34] Therefore, XANES is sensitive to the thickness-dependent chemical changes of phosphorene. However, the beam size commonly used for XANES is in the order of millimeters, which is not suitable for the spatial scale of phosphorene (around tens to hundreds of nanometers). To further improve the spatial resolution of XANES, synchrotron-based scanning transmission X-ray microscopy (STXM), which combining an undulator source and zone plate optics, is further considered to realize high spatial resolution, enabling nanoscale chemical imaging and absolute thickness measurements.[31,35]

In this work, we applied synchrotron-based STXM at the nanoscale resolution for the very first time (∼30 nm in this case), together with in situ synchrotron-based XPS (high energy resolution, high photon intensity, and high cross-section due to photon energy tunability) and XANES at the P K-edge to study the degraded phosphorene under the ambient condition.[36] Taking advantages of the morphology sensitivity of X-ray microscopy and the thickness and chemical sensitivity of XPS and XANES, the oxidation states of several regions corresponding to the thickness and the interaction between adjacent regions have been probed. By chemical mapping of degraded phosphorene at the nanoscale, the thickness effect and proximity effect have been obtained, clarifying the morphological effect on phosphorene degradation. The thinner regions are easier to be oxidized, and the already oxidized phosphorene tends to aggravate the degradation of the adjacent regions. In addition, based on the in situ XPS and XANES study of the phosphorene degradation, the oxidization process of phosphorene in air is revealed. Fresh phosphorene is initially oxidized to P(III) and then subsequently oxidized to P(V), and phosphorene oxidation starts from the surface and then spreads to the inside parts through the analysis of the averaged chemical states of phosphorene.

2. EXPERIMENTAL SECTION

2.1. Materials Preparation Method. *Phosphorene*: Similar to the previous report,[1] phosphorene [45 mg of Bulk BP (purchased from Smart Elements)] was immersed in 45 mL of *N*-methyl-2-pyrrolidone (NMP). Then, solution was then used for liquid exfoliation by tip-sonication (Qsonica Q700 sonicator) with the amplitude 80 for 1 h. Then, the as-prepared dispersions were centrifuged with the speed of 7000 rpm for 1 h to get the top half of the dispersion to obtain the phosphorene. The concentration of the obtained phosphorene solution is around 0.23 mg mL^{-1}.

2.2. Morphology Characterization. The morphology of the samples was characterized by Hitachi S-4800 field emission scanning electronic microscopy and JEOL 2010F field emission TEM. Raman spectra were obtained using a Horiba Scientific LabRAM HR Raman spectrometer system equipped with a 532.4 nm laser. AFM measurement was performed by means of the Park Systems XE-100 system.

2.3. X-ray Photoelectron Spectroscopy and X-ray Absorption Near-Edge Structure. The P 2p XPS spectra of phosphorene during degradation process under ambient condition were collected at the variable line spacing plane grating monochromator beamline. XPS measurements were performed immediately at a base pressure of $\sim 10^{-9}$ mbar. The excitation photon energy was set at 240 eV. The P K-edge XANES spectra of phosphorene and reference samples, including bulk BP and P_2O_5, were collected at the soft X-ray microcharacterization beamline (SXRMB) at the Canadian light source. One detection mode was used to get the XANES spectra, which is the fluorescence yield (FLY) mode. For the in situ XPS and XANES study of the phosphorene degradation process, the samples were degraded for different times, and the P 2p XPS and K-edge XANES spectra were acquired by focusing the beam at the same position. The humidity degree of ambient air for the in situ study is around 30−40%.

2.4. Scanning Transmission X-ray Microscopy. STXM measurement was conducted at the SM beamline of the Canadian light source (CLS), which is equipped with a 25 nm outermost-zone plate (CXRO, Berkeley Lab). The diffraction limited spatial resolution for this zone plate is 30 nm. The phosphorene samples were raster-scanned with synchronized detection of transmitted X-rays to generate images. Chemical imaging and XANES spectra are obtained using image sequence (stack) scans over a range of photon energies at the P K-edge. STXM data were analyzed using the aXis2000 software package (http://unicorn.mcmaster.ca/aXis2000.html), which allows for detailed interactive processing of the images and fitting of the X-ray absorption spectra. XANES from interesting locations were extracted from image stacks using the image mask which only selects the regions of interest (ROI). XANES from fresh phosphorene and fully oxidized regions were used as reference spectra for stack fitting to generate chemical component maps. The color composite map was created by combining individual component maps with the image intensity rescaled for better visualization. The humidity degree of ambient air for the ex situ STXM study is around 30−40%.

2.5. Comparison between SXRMB and SM Beamlines for P K-Edge XANES Spectra. The photon energy resolution of two beamlines near P K-edge (∼2152 eV) is different. Based on the beamline design, the photon energy resolution ($E/\Delta E$) of the SXRMB beamline is 10^4. Therefore, the energy resolution of SXRMB beamline near P K-edge is around 0.21 eV. At the SM beamline, the nominal photon energy resolution ($E/\Delta E$) is around 3000 and can reach $>10^4$. The energy resolution of the SM beamline we used to test STXM is around 0.7 eV. The lower energy resolution near the P K-edge at SM leads to the broader white line of P K-edge XANES of Pn compared with the result acquired at SXRMB beamline.

https://dx.doi.org/10.1021/acs.chemmater.9b04811
Chem. Mater. 2020, 32, 1272−1280

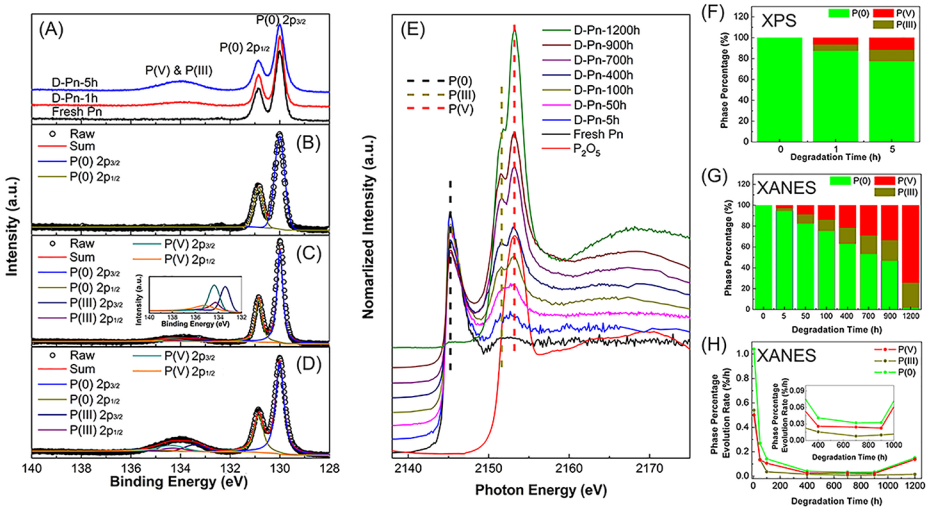

Figure 1. In situ synchrotron-based XPS and XANES study of phosphorene degradation under ambient condition. (A) P 2p XPS spectra and (B–D) curve fitting result of fresh phosphorene and degraded phosphorene for 1 and 5 h. (E) Normalized P K-edge XANES spectra of fresh phosphorene and degraded phosphorene for different time and the reference XANES spectra of P_2O_5. (F) Combination fitting result of in situ XPS spectra. (G) LCF result of in situ XANES, and (H) corresponding phase percentage evolution rate during in situ XANES study process.

3. RESULTS AND DISCUSSION

Phosphorene under investigation was prepared by liquid exfoliation of bulk BP in NMP via tip-sonication.[37] The purchased bulk BP shows the typical layered structure as shown in the SEM image and good crystal quality based on the X-ray diffraction pattern (see Supporting Information, Figure S1). Additionally, no impurity was found in the bulk BP, according to the energy-dispersive X-ray spectroscopy. The characterization results of the bulk BP confirm that it is one good precursor to be used to prepare phosphorene. To avoid degradation of phosphorene during the liquid exfoliation process, all procedures were carried out in an inert atmosphere (see Experimental Section for details). Figure S2 (see Supporting Information) displays the TEM and high-resolution TEM images of the phosphorene thus prepared. The phosphorene shows an ultrathin nanosheet morphology and a typical crystalline structure with a lattice spacing of 0.22 nm corresponding to the (014) crystal plane. The lattice structure of phosphorene indicates no obvious degradation, in accordance with the SEM of phosphorene (see Supporting Information, Figure S3). As shown in Figure S3, the phosphorene nanosheets range from around several hundred nanometers to several micrometers in size. To obtain the thickness information of the phosphorene nanosheet, AFM has been carried out, and the phosphorene ranges from 3 to 14 nm in thickness (see Supporting Information, Figure S4A), corresponding to the blue-shift and decreased intensity of Raman peaks (see Supporting Information, Figure S5).[15,38]

To understand the degradation process of phosphorene under ambient condition, in situ synchrotron-based XPS and XANES studies have been carried out to track the oxidation states of degraded phosphorene during the process (see Experimental Section for details). Synchrotron-based XPS spectra of fresh phosphorene (fresh-Pn) and degraded phosphorene for 1 and 5 h (D-Pn-1h and D-Pn-5h) are shown in Figure 1A. Owing to the excitation photon energy of 240.00 eV, the probing depth is just around 1 nm (escape depth of the P 2p photoelectrons), realizing high surface sensitivity of around a couple of BP atomic layers. In the case of fresh-Pn (Figure 1B), it shows the typical P 2p XPS spectra with one characteristic doublet belonging to the P $2p_{3/2}$ and $2p_{1/2}$ orbitals with the peak positions of 130.00 and 130.86 eV, respectively. The spin–orbit splitting of around 0.86 eV is an atomic characteristic of phosphorus atoms.[23] No other XPS peaks at higher binding energy means only phosphorus–phosphorus bonds in fresh-Pn without any oxidization. After degradation for 1 h under ambient condition, XPS peaks belonging to two oxidation states, P(III) and P(V), are found in D-Pn-1h, consistent with previous results (Figure 1C).[25,26] After another 4 h degradation, D-Pn-5h shows similar oxidation peaks with increased intensity, suggesting more extensive oxidation after longer degradation time (Figure 1D), which is further confirmed by in situ P K-edge XANES study conducted at the FLY mode. As shown in Figure 1E, in situ XANES of phosphorene degradation was carried out focusing the X-ray beam on the same area of phosphorene degraded for up to 1200 h. Fresh-Pn shows typical XANES spectra with the white line at around 2145.2 eV, which is related to the electron transition from the P 1s orbital to the unoccupied electronic states of P 3p character.[39] Compared with bulk BP, fresh-Pn shows the similar XANES spectra with the same edge position and similar white line intensity, indicating that liquid exfoliation process cannot change the electronic structure from bulk BP to Pn (see Supporting Information, Figure S6). After exposure to an ambient atmosphere for over 5 h, the degraded Pn(D-Pn) shows one peak belonging to fresh-Pn and two peaks centered at 2151.4 and 2153.3 eV belonging to two higher oxidation states. Compared with the reference spectra of P_2O_5 and phosphates (see Supporting Information, Figure S7), the oxidation states for the D-Pn are a mixture of P(0) and P(III) and P(V).[40] While the intensity of P(0) peaks gradually decreases with increasing degradation time, P(III) and P(V) peaks display an opposite tendency, meaning that longer degradation time leads to more extensive oxidation and to higher oxidation states.

To quantitatively analyze the phosphorene degradation process, in situ XPS and XANES results were fitted to find out the phase evolution (see Supporting Information, Figure S8).[41–43] As shown in Figure 1F, the combination fitting result

https://dx.doi.org/10.1021/acs.chemmater.9b04811
Chem. Mater. 2020, 32, 1272–1280

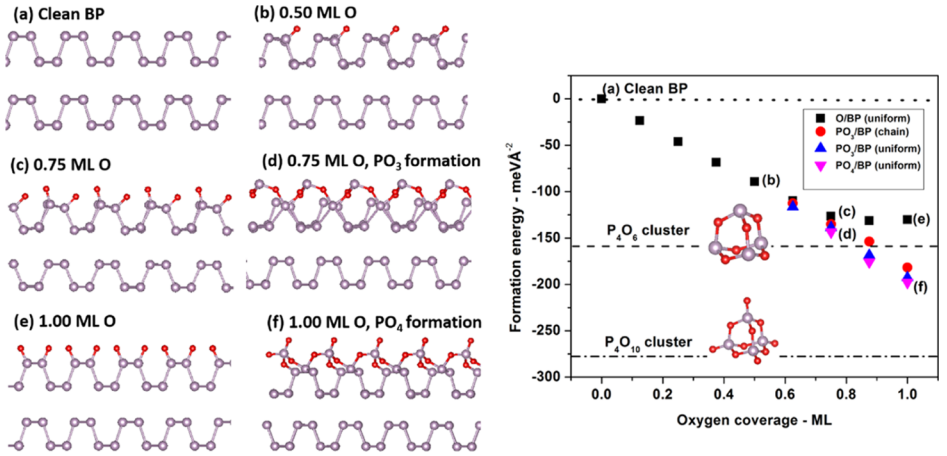

Figure 2. Calculated surface formation energies for various oxygen configurations on two-layer phosphorene as a function of oxygen coverage. Energies are relative to clean phosphorene and compared to the formation energies of P_4O_6 and P_4O_{10} clusters in the gas phase.

of XPS spectra shows the phase evolution at the surface (~1 nm), and the content of P(III) and P(V) increases with the degradation time, and the P(V) content (i.e., 6.4 and 11.5% at 1 and 5 h, respectively) is constantly higher than that of P(III) (i.e., 5.91 and 10.8% at 1 and 5 h, respectively). Similarly, the linear combination fitting (LCF) result of XANES spectra (Figure 1G) shows the mixture of P(III) and P(V) oxidation states in the XPS or XANES spectra, suggesting that both transformation processes from P(0) to P(III) and from P(III) to P(V) take place simultaneously.[43] However, the XANES spectra show different conclusion owing to the bulk sensitivity (several micro meters) of the FLY mode at the beginning of phosphorene degradation, lower P(III), and P(V) phase percentage (2.7 and 2.5%, respectively) after 5 h degradation. Additionally, the lower content of P(V) than P(III) is opposite from the XPS result. That means that the oxidation and degradation of phosphorene start from the surface and then spread to the bulk. The different intensity ratio of P(III) to P(V) at the surface and in the bulk suggests that phosphorene degradation is a two-step process. When phosphorene is exposed to ambient condition, P(III) is first formed, which is chemically unstable, and then transformed to P(V). At the surface, formed P(III) is easier to be further oxidized by oxygen. However, it is more difficult for the oxygen to go through the surface and then oxidize the formed P(III) in the bulk, leading to lower content of P(V) inside. After the initial degradation, the formation of P(III) also faces the oxygen-penetration problem. The content of P(V) starts to be higher than P(III). Based on the combination result after different degradation times, the phase evolution rate of P(0), P(III), and P(V) is calculated and shown in Figure 1H. The three phases show the similar rate evolution tendency, which goes down at the beginning and then goes up at the end. That means the initially formed oxidation surface layer blocks the contact between oxygen and phosphorene part, and the gradually increasing oxidation layer lowers down the degradation rate. However, the continuous degradation process finally leads to the collapse of crystal structure of entire phosphorene sheets, which promotes the degradation process together with the transformation from hydrophobic phosphorene to hydrophilic-oxidized phosphorene.[22] At the end of phosphorene, P(V) can be expected to be the highest oxidation state after complete degradation, consistent with previous reports.[14,17,19,26]

To further understand the oxidation mechanism of phosphorene, the VASP package[44] was used to carry out DFT calculations at the dispersion-corrected PBE-D3/zero level.[45] To simulate the BP surface, calculations under periodic boundary condition were performed on a two-layer BP slab. A vacuum space of 30 Å was added between repeated slab layers to minimize interactions between them. The surface formation energy was calculated as a function of oxygen coverage, which varies between zero and one monolayer (ML)

$$\gamma^{\mathrm{BPO}} = \frac{1}{2A}\left(E_{\mathrm{O/BP}} - NE_{\mathrm{BP/bulk}} - \frac{n}{2}E_{\mathrm{O_2}}\right) \quad (1)$$

where A is the unit-cell surface area, $E_{\mathrm{O/BP}}$ is the total energy of the oxygen-covered surface, $E_{\mathrm{BP/bulk}}$ is the calculated energy of BP in the bulk unit-cell, $E_{\mathrm{O_2}}$ is the energy of molecular oxygen in gas phase, N is the ratio of the number of P atoms in slab configuration to that in the bulk unit-cell, and n is the number of adsorbed O atoms.

The calculated surface formation energies are shown in Figure 2. For coverage below 0.5 ML, the most preferred adsorption site for O is the on-top dangling position (as shown in (a) and (b) in Figure 2). On the other hand, for coverage above 0.5 ML, adsorption on the dangling position is not energetically favored (as shown in (c) and (e) in Figure 2), and the surface undergoes structural reconstruction to form PO_3 and PO_4 groups. Upon this surface reconstruction, P atoms are displaced from their original position at the surface and become coordinated with three or four oxygen atoms (as shown in (d) and (f) in Figure 2 and see Supporting Information, Figure S12). The geometry of surface PO_3 groups is similar to that of phosphorus trioxide (P_4O_6), in which phosphorus atoms are coordinated with three O atoms. Similarly, the geometry of the PO_4 groups formed at higher oxygen coverage is analogues to the structure of phosphorus pentoxide (P_4O_{10}) in which the phosphorus atoms are bound by a tetrahedron of oxygen atoms. Thus, as also compared to the formation energies of P_4O_6 and P_4O_{10} clusters in Figure 2, theoretical results confirm the experimental findings of the two-step oxidation process of phosphorene that will eventually lead to the formation of P_2O_5. Furthermore, P_4O_6 and P_4O_{10} are susceptible to moisture absorption and will be transformed to corresponding phosphoric acid (i.e., H_3PO_3 and H_3PO_4). Our DFT results, thus, confirm the observation based on in

https://dx.doi.org/10.1021/acs.chemmater.9b04811
Chem. Mater. 2020, 32, 1272−1280

situ synchrotron-based XPS and XANES study, in which the oxidation mechanism of phosphorene under ambient condition proceeds as a two-step process. Fresh phosphorene is first oxidized to P(III) and further transformed to P(V) after prolonged degradation. Also, the oxidation starts from the surface and then spreads to the inside parts. Coordinates of the main structures are provided in the Supporting Information along with the surface energies calculated for various other terminations of O^{ad} on BP.[27]

Having revealed the chemical reaction during phosphorene degradation process, we study the morphology effect during the phosphorene degradation process using STXM, by studying the exact specimen on a TEM grid that had been investigated with TEM. As shown in Figure 3A, STXM is

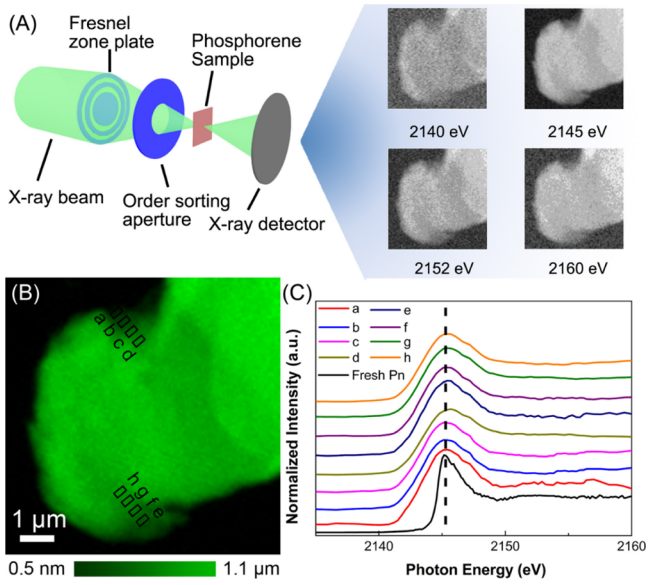

Figure 3. (A) Schematic illustration of the working principle of STXM at SM beamline, CLS and X-ray microscopy images of fresh phosphorene at several photon energies; (B) thickness map of fresh phosphorene derived from the P K-edge. The horizontal bar in (B) illustrates the green scale, representing the phosphorene thickness in nm. Based on the thickness distribution, several regions have been marked as a, b, c, d, e, f, g, and h, indicating the ROI. (C) Normalized P K-edge XANES spectra of the regions marked in (B) and fresh Pn.

conducted by focusing the beam with a Fresnel zone plate to a small spot and rasterizing over the phosphorene samples. It has strict thickness requirements for thickness measurements comparable to that of TEM. After collecting the X-ray microscopy images at a series of photon energies known as energy stacks (often as small steps, in tenth of an eV for example across the absorption edge of a specific element), the XANES spectra of each pixel can be obtained.[31] Additionally, the absolute thickness of phosphorene at each pixel can be acquired by fitting the XANES spectra with the quantitatively scaled reference spectra of fresh phosphorene (see Supporting Information, Figure S9A). The phosphorene thickness map determined at the P K-edge is displayed in Figure 3B, presenting the nanosheet morphology, in accordance with the TEM and SEM images (Figures S2 and S3). Based on the thickness distribution map, eight regions with different thicknesses (from 10 to 700 nm) have been selected to acquire the P K-edge XANES spectra, showing similar features compared with fresh BP and indicating no obvious oxidation peaks (Figure 3C). Although the absorption peak with the white line at around 2145.2 eV is consistent with the XANES spectrum of fresh-Pn, the broader white line is ascribed to the lower instrument energy resolution at the edge of energy range for the SXTM beamline.[39]

Then, the phosphorene was left in the ambient condition and degraded for a long time (30 days) to obtain oxidation information of prolong exposure, denoted as D-Pn-30d, and to study the degradation mechanism of phosphorene. As shown in Figure S8A (see Supporting Information), the nano-XANES spectrum acquired from the entire overall region of D-Pn-30d shows similar features compared with the XANES spectrum of D-Pn-700h shown in the above in situ XANES study. The broader peaks are also ascribed to the lower energy resolution for the SXTM beamline as noted above. However, the oxidation states in D-Pn-30d can be also interpreted as a mixture of P(0), P(III), and P(V). To further resolve the detailed composition of mixed oxidation states, XANES spectrum fitting was conducted as shown in Figure S8B (see Supporting Information).[41−43] Based on the XANES spectral fitting and composition fitting, the phase ratio of P(0), P(III), and P(V) is determined to be 6:3:1.

To quantitatively analyze the morphological effect during the degradation process of phosphorene, the thickness maps determined at the P K-edge of P(0), P(III) and P(V) are essential and they are presented in Figure 4A−C by

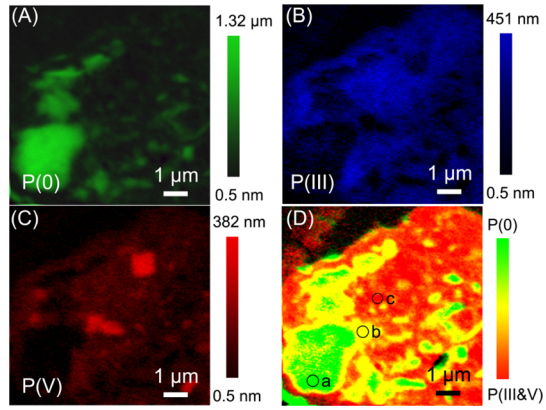

Figure 4. Thickness map derived from the P K-edge of (A) P(0), (B) P(III), and (C) P(V) in D-Pn-30d. The vertical bars in (A), (B), and (C) illustrate the green, blue, and red scales representing the thickness in nm. (D) Quasi-quantitative chemical phase map of D-Pn-30d (green: P(0), red: P(III and V). Three ROIs have been marked as a, b, and c.

conducting the P K-edge stack of D-Pn-30d fitting with the quantitatively scaled reference spectra of phosphorene and phosphoric acid (see Supporting Information, Figure S9A−C). Based on the thickness maps and XANES spectra, one quasi-quantitative intensity distribution map of P(0) and P(III and V) in D-Pn-30d is displayed in Figure 4D, which uses the broad peak corresponding to the mixture of P(III) and P(V) as the reference oxidation mixture spectra (see Supporting Information, Figures S8B and S9D). Compared with the AFM study of phosphorene degradation (see Supporting Information, Figure S4B), which just presents the morphology change without chemical information, STXM can provide detailed chemical imaging of degraded phosphorene. Three ROIs have been selected in Figure 5D, marked as a, b, and c, corresponding to the lowest, medium, and highest degree of

https://dx.doi.org/10.1021/acs.chemmater.9b04811
Chem. Mater. 2020, 32, 1272−1280

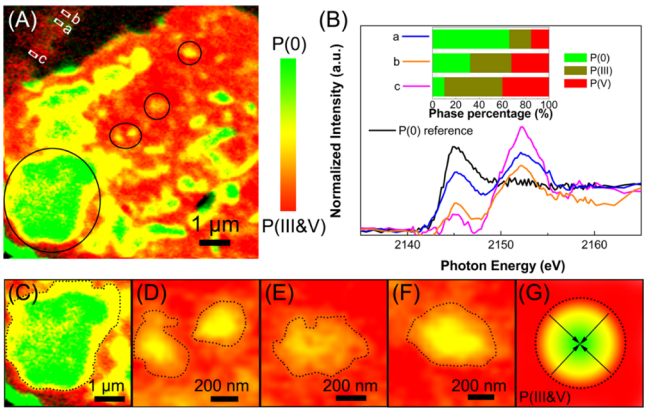

Figure 5. (A) Quasi-quantitative chemical phase map of D-Pn-30d [green: P(0), red: P(III and V)]. Several ROIs have been selected to understand the morphology effect. ROI a, b, and c have been selected to study the thickness effect, and other four regions marked with black circles are used to study the neighborhood effect. (B) Normalized P K-edge XANES spectra of the regions a, b, and c marked in (A), P^0, and P^{4+} with one inset of LCF result of each XANES spectrum. (C–F) Four regions have been marked black circles in (A) to understand the neighborhood effect, and (G) schematic illustration of the neighborhood effect.

oxidizations, respectively. The exact degree of oxidization of each ROI can be directly presented through the XANES spectra. As presented in Figure S10 (see Supporting Information), the XANES spectra of ROIs a, b, and c show gradual transformation to higher oxidation states with the increasing intensity of P(III and V) and decreasing intensity of P(0). Furthermore, ROIs a and c are dominated by P(0) and P(V) peaks, respectively, indicating that while ROI a just starts to be oxidized, the phosphorus in ROI c has been fully oxidized.

To get a better understanding of the morphological effect on the degradation process of phosphorene, ROIs with different thicknesses and surrounding environments of D-Pn-30d have been selected (i.e., ROIs a, b, and c), as shown in Figure 5A. Based on the thickness maps in Figure 4A–C, the thickness information of phosphorene and P(III) and P(V) oxides at the ROIs is listed in Table S1 (see Supporting Information), showing the thickness of a fresh phosphorene at these ROIs before degradation [(a) 9.8 nm; (b) 8.5 nm; (c) 4.7 nm]. Then, the chemical state of these ROIs is shown in Figure 5B, displaying a mixture of P(0), P(III), and P(V). Furthermore, the phase percentage of P(0), P(III), and P(V) in there ROIs is shown in the inset of Figure 5B, calculated based on the LCF (see Supporting Information, Figure S11). Comparing their ROIs, it is clear that the higher content of P(III) and P(V) is in the thinner phosphorene, meaning higher degree of oxidation. This result should be related to the thickness-dependent band structure, suggesting that the thickness effect plays a significant role in phosphorene degradation under ambient condition.[19]

In addition, based on the thickness variation result shown in Table S1 (see Supporting Information), degraded phosphorene shows increased thickness after the formation of P(III) and P(V) compared with fresh phosphorene, consistent with previous theoretical calculations and experimental results.[14,20] Moreover, the already oxidized regions are capable of increasing the local layer thickness and even resulting in cracking the crystal structure of neighborhood regions, accelerating the oxidization of phosphorene in theory, concluded as the proximity effect.[14] Up to now, the proximity effect has only been studied by the phenomenological modeling of IR s-SNOM result with no direct chemical

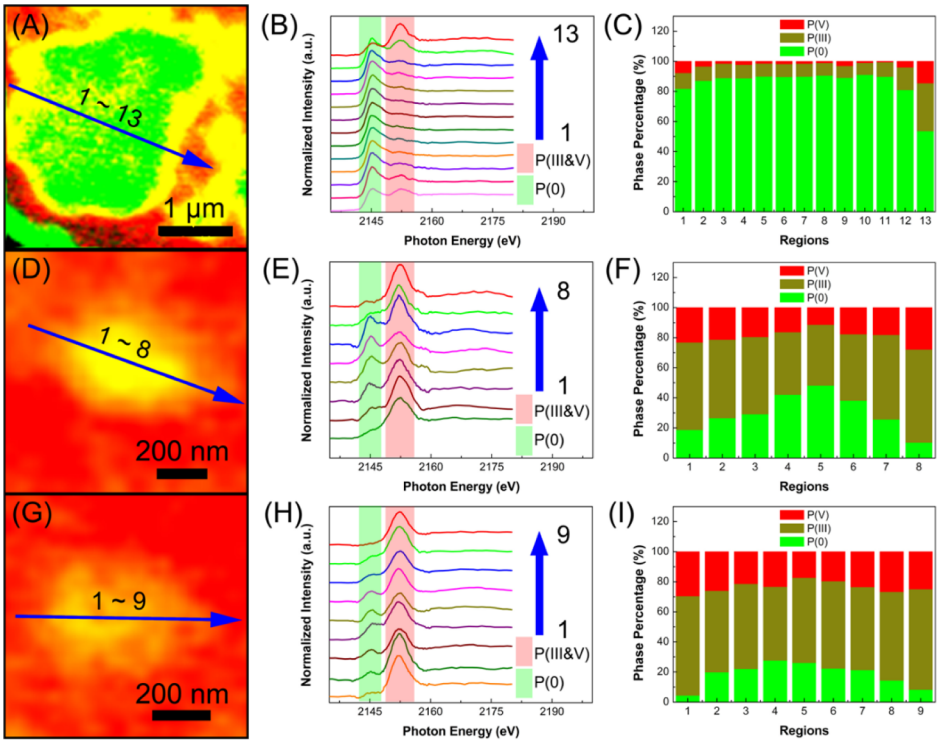

Figure 6. (A,D,G) Quasi-quantitative chemical phase map of several ROIs [green: P(0), red: P(III&V)]. (B,E,H) Normalized P K-edge XANES spectra and (C,F,I) LCF result of several parts marked by blue arrows in (A,D,G).

https://dx.doi.org/10.1021/acs.chemmater.9b04811
Chem. Mater. 2020, 32, 1272–1280

information.[20] Based on the STXM result displayed in Figure 5A, four RIOs have been marked with black circles as shown in Figure 5C−F. Each region marked with the dash line in Figure 5C−F displays the similar thickness of phosphorene. Based on the thickness effect discussed above, different areas in each region should show similar degree of oxidization. However, through comparing the phase combination images in each region, the areas near the edge, next to the adjacent highly oxidized regions, tends to be in higher oxidization states than the center parts away from the highly oxidized regions. This result indicates that the highly oxidized regions would promote the oxidization of the adjacent areas, and the neighborhood effect, as shown in the schematic illustration, is apparent (Figure 5G). Additionally, the unavoidable defects formed from the BP growth procedure and liquid exfoliation process can also accelerate the degradation process.[46] The proximity effect combined the defects leads to the irregular shape of degradation regions as shown in Figure 5C−F. The quantitative analysis result of the proximity effect in several regions is shown in Figure 6. Along with the blue arrows marked in Figure 6A,D,G, a series of gradually varied XANES spectra at the P K-edge are shown in Figure 6B,E,H. It is apparent from the edge to the center, the intensities of P(III and V) peaks gradually increase while the P(0) peaks gradually decrease, showing that the already oxidized regions will accelerate the oxidation of adjacent regions. This result is further confirmed by the LCF, as shown in Figure 6C,F,I, suggesting the obvious neighborhood effect during phosphorene degradation. Additionally, the normalized XANES spectra and LCF result of the overall regions marked in Figure 6A,D,G are shown in Figure S12 (see Supporting Information), showing that the thinner regions show higher degree of oxidization compared to the thicker ones.

Based on the above result and discussion, it is clear that the phosphorene degradation under ambient condition is a step-by-step process and starts from the surface to the inside parts. Initially, the thinner region of phosphorene is first oxidized under the impact of light and oxygen, which absorbs moisture and transforms to phosphoric acid. Then, the already oxidized regions in phosphorene increase the layer thickness and produce defects, accelerating the oxidation of adjacent regions. During the oxidization process, P(III) is first formed and then further oxidized to be P(V). With increasing degradation time, the content of P(III) and P(V) increases at the expense of P(0). Regarding the evolution of phosphorene degradation in the sheets, the degradation starts at the surface and the oxygen penetrate through the surface and oxidize the inside parts. The degradation rate decreases after the initial oxidation at the surface because of the block of oxygen penetration by the surface and then increases at the end, owing to the collapse of entire crystal structure and hydrophilic properties of phosphorene oxides. At the final degradation stage, phosphorene will be fully transformed to P(V) oxide.

4. CONCLUSIONS

We have, for the first time, provided a clear nanoscale chemical imaging of the morphology effect during phosphorene degradation under ambient condition using STXM and macroscopic specimens using in situ synchrotron-based XPS and XANES spectra. The high spatial and chemical resolution of STXM provides unprecedented morphology information (e.g., thickness and adjacent situation) and reveals the oxidation states of degraded phosphorene at any given region of interest. Through analyzing the effect of thickness and adjacent regions of degraded phosphorene, the thickness and proximity effects during phosphorene degradation clearly emerge from a chemical perspective: the thinner phosphorene is easier to be oxidized owing to the band structure, and the oxidized regions can accelerate the degradation of adjacent regions, which contribute to the phosphorene degradation process, simultaneously. Furthermore, the oxidization process of phosphorene was also studied by in situ XPS and XANES; the results show that the fresh phosphorene is first oxidized to be P(III) and then further oxidized to be P(V) in short time under the ambient condition. Additionally, the oxidation starts at the surface and then spread to the inside parts, resulting the fully oxidized state at last. Thus, a better understanding of the morphology effect during phosphorene degradation has been achieved in this work using a combination of synchrotron-based STXM, XPS, and XANES techniques, which will facilitate the development of phosphorene, especially the protection strategies.

■ ASSOCIATED CONTENT

Supporting Information

The Supporting Information is available free of charge at https://pubs.acs.org/doi/10.1021/acs.chemmater.9b04811.

Additional information and figures about bulk BP, phosphorene, and the theoretical study (PDF)

■ AUTHOR INFORMATION

Corresponding Authors

Tsun-Kong Sham − *Department of Chemistry and Soochow-Western Centre for Synchrotron Radiation Research, University of Western Ontario, London N6A 5B7, Canada;* orcid.org/0000-0003-1928-6697; Phone: +1-519-661-2111 ext 86341; Email: tsham@uwo.ca

Xueliang Sun − *Department of Mechanical and Materials Engineering, University of Western Ontario, London N6A 5B9, Canada;* orcid.org/0000-0003-0374-1245; Phone: +1-519-661-2111 ext 87759; Email: xsun9@uwo.ca

Authors

Weihan Li − *Department of Mechanical and Materials Engineering and Department of Chemistry and Soochow-Western Centre for Synchrotron Radiation Research, University of Western Ontario, London N6A 5B9, Canada*

Zhiqiang Wang − *Department of Chemistry and Soochow-Western Centre for Synchrotron Radiation Research, University of Western Ontario, London N6A 5B7, Canada;* orcid.org/0000-0003-0628-5222

Feipeng Zhao − *Department of Mechanical and Materials Engineering, University of Western Ontario, London N6A 5B9, Canada*

Minsi Li − *Department of Mechanical and Materials Engineering and Department of Chemistry and Soochow-Western Centre for Synchrotron Radiation Research, University of Western Ontario, London N6A 5B9, Canada*

Xuejie Gao − *Department of Mechanical and Materials Engineering and Department of Chemistry and Soochow-Western Centre for Synchrotron Radiation Research, University of Western Ontario, London N6A 5B9, Canada*

Yang Zhao − *Department of Mechanical and Materials Engineering, University of Western Ontario, London N6A 5B9, Canada*

Jian Wang − *Canadian Light Source, Saskatoon S7N 2V3, Canada*
Jigang Zhou − *Canadian Light Source, Saskatoon S7N 2V3, Canada;* orcid.org/0000-0001-6644-2862
Yongfeng Hu − *Canadian Light Source, Saskatoon S7N 2V3, Canada*
Qunfeng Xiao − *Canadian Light Source, Saskatoon S7N 2V3, Canada*
Xiaoyu Cui − *Canadian Light Source, Saskatoon S7N 2V3, Canada*
Mohammad Javad Eslamibidgoli − *Department of Chemistry, Simon Fraser University, Burnaby V5A 1S6, Canada*
Michael. H. Eikerling − *Department of Chemistry, Simon Fraser University, Burnaby V5A 1S6, Canada*
Ruying Li − *Department of Mechanical and Materials Engineering, University of Western Ontario, London N6A 5B9, Canada*
Frank Brandys − *3M Canada Company, London N5V 3R6, Canada*
Ranjith Divigalpitiya − *3M Canada Company, London N5V 3R6, Canada*

Complete contact information is available at: https://pubs.acs.org/10.1021/acs.chemmater.9b04811

Author Contributions

W.L., Z.W., and F.Z. contributed equally to this work. M.J.E. and M.H.E. contributed in the theoretical study of this work.

Notes

The authors declare no competing financial interest.

■ ACKNOWLEDGMENTS

This work was funded by the Nature Sciences and Engineering Research Council of Canada (NSERC), the Canada Research Chair Program, the Canada Foundation for Innovation (CFI), 3M Canada, the Ontario Research Fund, the Canada Light Source (CLS) at the University of Saskatchewan, and the University of Western Ontario. CLS was supported by CFI, NSERC, NRC, CHIR, and the University of Saskatchewan. M.L. and X.G. thank the China Scholarship Council (CSC) for the financial support. W.L., Z.W., F.Z., M.L. and X.G. acknowledge the receipt of support from the CLSI Graduate and Post-Doctoral Student Travel Support Program. We also appreciate the help of the beamline scientists of Beamline 9-BM at Advanced Photon Source, Dr. Tianpin Wu and Dr. Lu Ma. We also thank Prof. Gianluigi Botton, Dr. Hanshuo Liu, and Andrei Carmen in McMaster University for the help and support.

■ REFERENCES

(1) Bridgman, P. W. Two New Modifications of Phosphorus. *J. Am. Chem. Soc.* **1914**, *36*, 1344−1363.
(2) Carvalho, A.; Wang, M.; Zhu, X.; Rodin, A. S.; Su, H.; Neto, A. H. C. Phosphorene: from theory to applications. *Nat. Rev. Mater.* **2016**, *1*, 16061.
(3) Li, L.; Yu, Y.; Ye, G. J.; Ge, Q.; Ou, X.; Wu, H.; Feng, D.; Chen, X. H.; Zhang, Y. Black phosphorus field-effect transistors. *Nat. Nanotechnol.* **2014**, *9*, 372.
(4) Ling, X.; Wang, H.; Huang, S.; Xia, F.; Dresselhaus, M. S. The renaissance of black phosphorus. *Proc. Natl. Acad. Sci. U.S.A.* **2015**, *112*, 4523−4530.
(5) Tran, V.; Soklaski, R.; Liang, Y.; Yang, L. Layer-controlled band gap and anisotropic excitons in few-layer black phosphorus. *Phys. Rev. B: Condens. Matter Mater. Phys.* **2014**, *89*, 235319.
(6) Li, L.; Kim, J.; Jin, C.; Ye, G. J.; Qiu, D. Y.; da Jornada, F. H.; Shi, Z.; Chen, L.; Zhang, Z.; Yang, F.; Watanabe, K.; Taniguchi, T.; Ren, W.; Louie, S. G.; Chen, X. H.; Zhang, Y.; Wang, F. Direct observation of the layer-dependent electronic structure in phosphorene. *Nat. Nanotechnol.* **2017**, *12*, 21.
(7) Qiao, J.; Kong, X.; Hu, Z.-X.; Yang, F.; Ji, W. High-mobility transport anisotropy and linear dichroism in few-layer black phosphorus. *Nat. Commun.* **2014**, *5*, 4475.
(8) Jang, H.; Wood, J. D.; Ryder, C. R.; Hersam, M. C.; Cahill, D. G. Anisotropic thermal conductivity of exfoliated black phosphorus. *Adv. Mater.* **2015**, *27*, 8017−8022.
(9) Luo, Z.; Maassen, J.; Deng, Y.; Du, Y.; Garrelts, R. P.; Lundstrom, M. S.; Peide, D. Y.; Xu, X. Anisotropic in-plane thermal conductivity observed in few-layer black phosphorus. *Nat. Commun.* **2015**, *6*, 8572.
(10) Xia, F.; Wang, H.; Jia, Y. Rediscovering black phosphorus as an anisotropic layered material for optoelectronics and electronics. *Nat. Commun.* **2014**, *5*, 4458.
(11) Fei, R.; Yang, L. Strain-engineering the anisotropic electrical conductance of few-layer black phosphorus. *Nano Lett.* **2014**, *14*, 2884−2889.
(12) Xue, Y.; Zhang, Q.; Zhang, T.; Fu, L. Black Phosphorus: Properties, Synthesis, and Applications in Energy Conversion and Storage. *ChemNanoMat* **2017**, *3*, 352−361.
(13) Ziletti, A.; Carvalho, A.; Trevisanutto, P.; Campbell, D.; Coker, D.; Neto, A. C. Phosphorene oxides: Bandgap engineering of phosphorene by oxidation. *Phys. Rev. B: Condens. Matter Mater. Phys.* **2015**, *91*, 085407.
(14) Ziletti, A.; Carvalho, A.; Campbell, D. K.; Coker, D. F.; Neto, A. C. Oxygen defects in phosphorene. *Phys. Rev. Lett.* **2015**, *114*, 046801.
(15) Castellanos-Gomez, A.; Vicarelli, L.; Prada, E.; Island, J. O.; Narasimha-Acharya, K. L.; Blanter, S. I.; Groenendijk, D. J.; Buscema, M.; Steele, G. A.; Alvarez, J. V.; Zandbergen, H. W.; Palacios, J. J.; van der Zant, H. S. J. Isolation and characterization of few-layer black phosphorus. *2D Mater.* **2014**, *1*, 025001.
(16) Island, J. O.; Steele, G. A.; Zant, H. S. J. v. d.; Castellanos-Gomez, A. Environmental instability of few-layer black phosphorus. *2D Mater.* **2015**, *2*, 011002.
(17) Favron, A.; Gaufrès, E.; Fossard, F.; Phaneuf-L'Heureux, A.-L.; Tang, N. Y.-W.; Lévesque, P. L.; Loiseau, A.; Leonelli, R.; Francoeur, S.; Martel, R. Photooxidation and quantum confinement effects in exfoliated black phosphorus. *Nat. Mater.* **2015**, *14*, 826.
(18) Ahmed, T.; Balendhran, S.; Karim, M. N.; Mayes, E. L.; Field, M. R.; Ramanathan, R.; Singh, M.; Bansal, V.; Sriram, S.; Bhaskaran, M. Degradation of black phosphorus is contingent on UV−blue light exposure. *npj 2D Mater. Appl.* **2017**, *1*, 18.
(19) Zhou, Q.; Chen, Q.; Tong, Y.; Wang, J. Light-induced ambient degradation of few-layer black phosphorus: mechanism and protection. *Angew. Chem., Int. Ed.* **2016**, *55*, 11437−11441.
(20) Gamage, S.; Li, Z.; Yakovlev, V. S.; Lewis, C.; Wang, H.; Cronin, S. B.; Abate, Y. Nanoscopy of black phosphorus degradation. *Adv. Mater. Interfaces* **2016**, *3*, 1600121.
(21) Wood, J. D.; Wells, S. A.; Jariwala, D.; Chen, K.-S.; Cho, E.; Sangwan, V. K.; Liu, X.; Lauhon, L. J.; Marks, T. J.; Hersam, M. C. Effective passivation of exfoliated black phosphorus transistors against ambient degradation. *Nano Lett.* **2014**, *14*, 6964−6970.
(22) Huang, Y.; Qiao, J.; He, K.; Bliznakov, S.; Sutter, E.; Chen, X.; Luo, D.; Meng, F.; Su, D.; Decker, J.; Ji, W.; Ruoff, R. S.; Sutter, P. Interaction of black phosphorus with oxygen and water. *Chem. Mater.* **2016**, *28*, 8330−8339.
(23) Edmonds, M. T.; Tadich, A.; Carvalho, A.; Ziletti, A.; O'Donnell, K. M.; Koenig, S. P.; Coker, D. F.; Özyilmaz, B.; Neto, A. H. C.; Fuhrer, M. S. Creating a stable oxide at the surface of black phosphorus. *ACS Appl. Mater. Interfaces* **2015**, *7*, 14557−14562.
(24) Luo, W.; Zemlyanov, D. Y.; Milligan, C. A.; Du, Y.; Yang, L.; Wu, Y.; Ye, P. D. Surface chemistry of black phosphorus under a controlled oxidative environment. *Nanotechnology* **2016**, *27*, 434002.

(25) Zhang, T.; Wan, Y.; Xie, H.; Mu, Y.; Du, P.; Wang, D.; Wu, X.; Ji, H.; Wan, L. Degradation Chemistry and Stabilization of Exfoliated Few-Layer Black Phosphorus in Water. *J. Am. Chem. Soc.* **2018**, *140*, 7561−7567.
(26) Wang, Y.; Yang, B.; Wan, B.; Xi, X.; Zeng, Z.; Liu, E.; Wu, G.; Liu, Z.; Wang, W. Degradation of black phosphorus: a real-time 31P NMR study. *2D Mater.* **2016**, *3*, 035025.
(27) Eslamibidgoli, M. J.; Eikerling, M. H. Mechanical and Chemical Stability of Monolayer Black Phosphorous Studied by Density Functional Theory Simulations. *J. Phys. Chem. C* **2018**, *122*, 22366−22373.
(28) Abellán, G.; Wild, S.; Lloret, V.; Scheuschner, N.; Gillen, R.; Mundloch, U.; Maultzsch, J.; Varela, M.; Hauke, F.; Hirsch, A. Fundamental Insights into the Degradation and Stabilization of Thin Layer Black Phosphorus. *J. Am. Chem. Soc.* **2017**, *139*, 10432−10440.
(29) Goode, A. E.; Porter, A. E.; Ryan, M. P.; McComb, D. W. Correlative electron and X-ray microscopy: probing chemistry and bonding with high spatial resolution. *Nanoscale* **2015**, *7*, 1534−1548.
(30) Lin, F.; Liu, Y.; Yu, X.; Cheng, L.; Singer, A.; Shpyrko, O. G.; Xin, H. L.; Tamura, N.; Tian, C.; Weng, T.-C.; Yang, X.-Q.; Meng, Y. S.; Nordlund, D.; Yang, W.; Doeff, M. M. Synchrotron X-ray analytical techniques for studying materials electrochemistry in rechargeable batteries. *Chem. Rev.* **2017**, *117*, 13123−13186.
(31) Wang, L.; Wang, J.; Zuo, P. Probing Battery Electrochemistry with In Operando Synchrotron X-Ray Imaging Techniques. *Small Methods* **2018**, *2*, 1700293.
(32) Huang, W.; Marcelli, A.; Xia, D. *Application of Synchrotron Radiation Technologies to Electrode Materials for Li- and Na-Ion Batteries*; Advanced Energy Materials, 2017, *7*, 1700460.
(33) Wang, J.; Zhou, J.; Hu, Y.; Regier, T. Chemical interaction and imaging of single Co 3 O 4/graphene sheets studied by scanning transmission X-ray microscopy and X-ray absorption spectroscopy. *Energy Environ. Sci.* **2013**, *6*, 926−934.
(34) Zhou, J. G.; Wang, J.; Sun, C. L.; Maley, J. M.; Sammynaiken, R.; Sham, T. K.; Pong, W. F. Nano-scale chemical imaging of a single sheet of reduced graphene oxide. *J. Mater. Chem.* **2011**, *21*, 14622−14630.
(35) Sakdinawat, A.; Attwood, D. Nanoscale X-ray imaging. *Nat. Photonics* **2010**, *4*, 840.
(36) Kaznatcheev, K. V.; Karunakaran, C.; Lanke, U. D.; Urquhart, S. G.; Obst, M.; Hitchcock, A. P. Soft X-ray spectromicroscopy beamline at the CLS: commissioning results. *Nucl. Instrum. Methods Phys. Res., Sect. A* **2007**, *582*, 96−99.
(37) Kang, J.; Wood, J. D.; Wells, S. A.; Lee, J.-H.; Liu, X.; Chen, K.-S.; Hersam, M. C. Solvent exfoliation of electronic-grade, two-dimensional black phosphorus. *ACS Nano* **2015**, *9*, 3596−3604.
(38) Guo, Z.; Zhang, H.; Lu, S.; Wang, Z.; Tang, S.; Shao, J.; Sun, Z.; Xie, H.; Wang, H.; Yu, X.-F.; Chu, P. K. From black phosphorus to phosphorene: basic solvent exfoliation, evolution of Raman scattering, and applications to ultrafast photonics. *Adv. Funct. Mater.* **2015**, *25*, 6996−7002.
(39) Nicotra, G.; Politano, A.; Mio, A. M.; Deretzis, I.; Hu, J.; Mao, Z. Q.; Wei, J.; La Magna, A.; Spinella, C. Absorption edges of black phosphorus: A comparative analysis. *Phys. Status Solidi B* **2016**, *253*, 2509−2514.
(40) Prietzel, J.; Thieme, J.; Paterson, D. Phosphorus speciation of forest-soil organic surface layers using PK-edge XANES spectroscopy. *J. Plant Nutr. Soil Sci.* **2010**, *173*, 805−807.
(41) Küper, G.; Chauvistré, R.; Hormes, J.; Frick, F.; Jansen, M.; Lüer, B.; Hartmann, E. Phosphorus K shell photoabsorption spectra of the oxides P4O6, P4O10, P (C6H5O) 3 and PO (C6H5O) 3. *Chem. Phys.* **1992**, *165*, 405−414.
(42) Ingall, E. D.; Brandes, J. A.; Diaz, J. M.; de Jonge, M. D.; Paterson, D.; McNulty, I.; Elliott, W. C.; Northrup, P. Phosphorus K-edge XANES spectroscopy of mineral standards. *J. Synchrotron Radiat.* **2011**, *18*, 189−197.
(43) Ravel, B.; Newville, M. ATHENA, ARTEMIS, HEPHAESTUS: data analysis for X-ray absorption spectroscopy using IFEFFIT. *J. Synchrotron Radiat.* **2005**, *12*, 537−541.
(44) Kresse, G.; Furthmüller, J. Efficient iterative schemes for ab initio total-energy calculations using a plane-wave basis set. *Phys. Rev. B: Condens. Matter Mater. Phys.* **1996**, *54*, 11169.
(45) Grimme, S.; Antony, J.; Ehrlich, S.; Krieg, H. A consistent and accurate ab initio parametrization of density functional dispersion correction (DFT-D) for the 94 elements H-Pu. *J. Chem. Phys.* **2010**, *132*, 154104.
(46) Utt, K. L.; Rivero, P.; Mehboudi, M.; Harriss, E. O.; Borunda, M. F.; Pacheco SanJuan, A. A.; Barraza-Lopez, S. Intrinsic defects, fluctuations of the local shape, and the photo-oxidation of black phosphorus. *ACS Cent. Sci.* **2015**, *1*, 320−327.

https://dx.doi.org/10.1021/acs.chemmater.9b04811
Chem. Mater. 2020, 32, 1272−1280